White light-emitting electrochemical cells based on deep-red Cu(I) complexes

Elisa Fresta,[1,2] Michael D. Weber,[3] Julio Fernández-Cestau[1] and Rubén D. Costa[1,3]*

[1]IMDEA Materials Institute, Calle Eric Kandel 2, E-28906 Getafe, Madrid, Spain.

[2]Department of Applied Physics, Faculty of Science M12, Universidad Autónoma de Madrid, 28049 Madrid,Spain

[3]Department of Chemistry and Pharmacy, Chair of Physical Chemistry I, University of Erlangen-Nürnberg, Egerlandstrasse 3, 91058, Erlangen, Germany

KEYWORDS: Thin film lighting, light-emitting electrochemical cells, white-emitting devices, deep-red emitters, copper (I) complexes

ABSTRACT: The synthesis, characterization and photoluminescent and electrochemical features of ionic Copper(I) coordination complexes, i.e., $[Cu(N^N)(P^P)]^+$, where N^N is 4,4'-diethylester-2,2'-biquinoline (dcbq) and P^P is bis-triphenylphosphine, bis[2-(diphenylphosphino)phenyl)ether] (POP) or 4,5-Bis(diphenylphosphino)-9,9-dimethylxanthene (Xantphos), are reported along with their application to achieve both deep-red and white LECs. Precisely, are achieved deep-red emitting devices with high irradiances of up to 97.9 $\mu W/cm^2$ long stabilities of up to 21 h and excellent colour stability resulting in Commission Internationale de

l'Éclairage 1931 (CIE) color coordinates x/y of 0.66/0.32. This represents the first Cu(I)-based deep-red emitting LEC. More important, we shed light on the electroluminescent behavior with respect to the irradiance, light output, colour quality and stability, as well as the impact of introducing an ionic liquid as a supporting electrolyte. We rationalized these results to photophysical and electrochemical studies that supports the trend obtained in lighting devices. Finally, by using a wide band-gap material, we manufacture a white-emitting device with CIE 1931 colour coordinates of x/y of 0.31/0.32 and a high color rendering index (CRI) of 92.

INTRODUCTION

One of the main challenges in solid-state lighting (SSL) technologies is the exploration of stable and sustainable efficient emitters for large area lighting applications.[1] To tackle current limitations a viable approach is to implement low-cost earth-abundant materials- *e.g.* copper[2–11] –in single-layer thin-film lighting devices for developing good performing light-emitting electrochemical cells (LECs).[12–14]

LECs consist of an ionic-based active layer sandwiched between electrodes.[15] In their preparation, having access to solution-based coating protocols significantly reduce fabrication time and costs.[16–18] For this reason, the use of soluble ionic transition metal complexes (iTMCs) as emitters has been intensively investigated throughout the last decade.[15,19,20] However, up to date, the most efficient devices are based in Ir(III)-iTMCs.[15,21–25] While these emitters span the whole visible range,[15,26,27] the high cost and low abundance of iridium in the Earth's crust,[28] do not match the future needs for large area and sustainable lighting. In this context, Cu(I)-iTMCs represent an appealing alternative to Ir(III)-iTMCs for LECs. Indeed, copper resources are abundant and considered as low-cost, and Cu(I)-iTMCs chemistry is well-known in literature,[29,30] allowing to tailor the features of the emitter, *e.g.*, the redox stability, the enhancement of the photoluminescence quantum yield (PLQY), and/or the shift of the luminescent response in the device, which recently led to major breakthroughs in LECs.[15,31]

As in early works on Ir(III)-iTMCs based LECs,[32] one of the major challenge is to identify possible complexes whose luminescent response covers the whole visible range. This has to be complemented with the right balance between efficiency, brightness, and stability, in order to

achieve well-performing white LECs in the near future.[33–35] In contrast to Ir, Cu-iTMCs LECs state-of-the-art involves yellow and blue-emitting complexes. In short, Costa *et al.* explored the possibility to prepare heteroleptic blue-emitting compounds with N^N ligands with high energy lowest unoccupied molecule orbital (LUMO) levels, achieving yellow-emitting devices due to the lack of a thermally activated delayed fluorescence (TADF) process.[36] However, the same authors proposed to use another family of Cu(I) complexes bearing different *N*-heterocyclic carbenes and dipyridylamine ligands-*i.e.* di-iso-propylphenyl)imidazole-2-ylidene and 2,2′ -bis-(3-methylpyridyl)amine, showing an effective TADF emission that led to the first blue-emitting Cu(I)-iTMC LECs.[37–39] Other studies by Zhang *et al.,*[40] Bolink *et al.*,[41–43] and Costa *et al.*[44–46] showed green- and yellowish-orange-emitting Cu(I)-based devices by changing the pattern substitution of heteroleptic diamine and diphosphine ligands.

Thus, deep red-emitting LECs based on Cu(I)-iTMCs are still missing, hampering the preparation of white-emitting LECs. Herein, we report the synthesis and the application of a series of deep-red emitting heteroleptic [Cu(N^N)(P^P)](PF_6) complexes. The complexes have the same N^N ligand, namely dcbq (= 4,4'-diethylester-2,2'-biquinoline), and different P^P ligands; $(PPh_3)_2$, POP (bis(2-(diphenylphosphino)phenyl)ether), and Xantphos (4,5-Bis(diphenylphosphino)-9,9-dimethylxanthene), named **1**, **2** and **3**, respectively, in the paper. The rigidity of the P^P ligand increases from **1** to **3**. As the rigidity increases, so it does the chemical stability and the non-radiative deactivation pathways related to a structural flattening in the emitting excited state decreases. For these reasons, complex **3** is the best candidate for LECs implementation.

The optimized LECs based on **3** feature deep-red-emitting efficient and stable devices achieving irradiances of 97.9 $\mu W/cm^2$ (x/y 0.66/0.32, λ_{max} 671 nm) and stabilities up to 21h. To the best of our knowledge, this is the first example of deep-red-emitting LEC based on the heteroleptic $[Cu(N^N)(P^P)]^+$ complexes. We further changed the chromaticity of the devices towards white LECs using a host: guest system comprising a hole transporting material (HTM) as host, namely 4,4′-bis(N-carbazolyl)-1,1′-biphenyl (CBP), and **3** as guest. The optimized device showed white light peaking at 379 nm, 478 nm and 653 nm, x/y CIE coordinates of 0.31/0.32 and CRI of 92.

EXPERIMENTAL SECTION

Synthesis and characterization

When required, manipulations were performed using standard Schlenk techniques under dry argon or using an M. Braun glove box. Solvents were obtained from a solvent purification system (M-BRAUN MB SPS-800). All commercial chemicals were used without further purification. Elemental analyses were carried out with a Carlo Erba EA1110 CHNS-O microanalyzer. NMR spectra were recorded on a Bruker ARX 300 spectrometers at 298 K. Chemical shifts are reported in parts per million (ppm) relative to external standards, and all coupling constants are given in hertz (Hz). Mass spectra were recorded on a Micromass ZABspec spectrometer utilizing electrospray ionization with a MeOH or CH_3CN mobile phase.

The ligand 4,4'-diethylester-2,2'-bipyridine was prepared as reported in reference[47]. Briefly, at 0ºC sulfuric acid in excess (20 mL) was dropwise added to 4,4'-dicarboxylic acid-2,2'-biquinoline (6 g, 17 mmol) in ethanol (80 mL). The reaction mixture was heated to reflux temperature overnight. The grey mixture was neutralized with NaOH (aq. 25 %) and the grey precipitate obtained filtered, washed with water and cold EtOH and air dried. ^{1}H NMR (300 MHz, $CDCl_3$) δ 9.31 (s, 2H), 8.80 (dd, J = 8.6, 1.5 Hz, 2H), 8.33 (dd, J = 8.4, 1.4 Hz, 2H), 7.84 (ddd, J = 8.4, 6.9, 1.5 Hz, 2H), 7.70 (ddd, J = 8.4, 6.9, 1.4 Hz, 2H), 4.60 (q, J = 7.1 Hz, 4H), 1.55 (t, J = 7.2 Hz, 6H).

[Cu(dcbq)(PPh_3)$_2$](PF_6) (1).

[Cu($NCCH_3$)$_4$](PF_6) (100 mg, 0.26 mmol) and PPh_3 (136 mg, 0.52 mmol) are mixed in 10 mL of dry CH_2Cl_2 and the reaction mixture stirred at room temperature for 20 min. After this time, dcbq (107 mg, 0.26 mmol) was added, what causes a noticeable colour change from colourless to dark red. The mixture was filtered through celite and the filtrate concentrated to ca. 2 mL by rotatory evaporation. The addition of diethyl ether caused the precipitation of a dark red solid that was filtered, washed with diethylether and dried under vacuum to give **1** (225 mg, 77 %). Anal. Calcd. For $C_{60}H_{50}N_2CuF_6O_4P_3$ (1133.51): C, 63.58; H, 4.45; N, 2.47. Found: C, 63.71; H, 4.57; N, 2.43. TOF-MS (ES+): [M]+ m/z = 987.2 , calculated m/z = 987.25. ^{1}H NMR (300 MHz, $CDCl_3$, 298K) (only signals attributed to **1** are given) δ 8.95 (s, 2H, H^3, dcbq), 8.72 (br, d, 2H, dcbq), 8.03 (br, m, 2H, dcbq), 7.66 (br, m, 2H, dcbq), 7.38 (br, t, 6H, PPh_3 + 2H, dcbq), 7.17 (br, m, 12H, PPh_3), 7.05 (br, m, 12H, PPh_3), 4.68 (br, q, 4H, CH_2, dcbq), 1.58 (br, t, 6H, dcbq). ^{31}P{^{1}H} NMR (121.5 MHz, $CDCl_3$, 298K): -2.02 (br, 2P, PPh_3), -144.27 (sept, 1P, PF_6, ^1J(P-F) = 712 Hz).

[Cu(dcbq)(POP)](PF_6) (2).

This complex was prepared following the same procedure described for **1**, but starting from [Cu($NCCH_3$)$_4$](PF_6) (100 mg, 0.26 mmol), POP (140 mg, 0.26 mmol) and dcbq (107 mg, 0.26

mmol). Complex **2** was isolated as a red solid (264 mg, 88%). Anal. Calcd. For $C_{60}H_{48}N_2CuF_6O_5P_3$ (1147.49): C, 62.80; H, 4.22; N, 2.44. Found: C, 62.71; H, 4.27; N, 2.42. TOF-MS (ES+): [M]+ m/z = 1001.2, calculated m/z = 1001.23. ^{1}H NMR (300 MHz, $CDCl_3$, 298K) δ 8.70 (d, *J* = 8.5 Hz, 2H, POP), 8.65 (s, 2H, H^3, dcbq), 8.41 (d, *J* = 8.6 Hz, 2H, dcbq), 7.63 (m, 2H, dcbq), 7.45–7.37 (m, 2H), 7.23 (br, t, 2H), 7.22-7.19 (m, 4H), 7.18-7.10 (m, 6H), 6.91 (br, dd, 8H, POP), 6.79 (br, dd, 8H, POP), 4.65 (q, ^3J = 7.2 Hz, 4H, CH_2, dcbq), 1.56 (t, ^3J = 7.2 Hz, 6H, CH_3, dcbq). ^{31}P{^{1}H} NMR (121.5 MHz, $CDCl_3$, 298K): -10.66 (br, 2P, POP), -144.28 (sept, 1P, PF_6, , ^1J(P-F) = 712 Hz).

[Cu(dcbq)(POP)](PF$_6$) (3).

This complex was prepared following the same procedure described for **1**, but starting from $[Cu(NCCH_3)_4](PF_6)$ (100 mg, 0.26 mmol), Xantphos (150 mg, 0.26 mmol) and dcbq (107 mg, 0.26 mmol). Complex **3** was isolated as a red solid (250 mg, 81 %). Anal. Calcd. For $C_{63}H_{52}CuF_6N_2O_5P_3$ (1187.55): C, 63.72; H, 4.41; N, 2.36. Found: C, 63.74; H, 4.47; N, 2.35. TOF-MS (ES+): [M]+ m/z = 1041.2, calculated m/z = 1041.26. ^{1}H NMR (300 MHz, $CDCl_3$, 298K) δ 8.86 (s, 2H, H^3, dcbq), 8.73 (d, *J* = 8.6 Hz, 2H, dcbq), 7.96 (d, *J* = 8.5 Hz, 2H), 7.75 (d, *J* = 7.8 Hz, 2H), 7.61 (t, *J* = 7.7 Hz, 2H), 7.32-7.26 (m, 4H), 7.14-7.06 (m, 10H), 7.01 (m, 2H), 4.67 (q, J = 7.1 Hz, 4H, CH_2, dcbq), 1.90 (s, 6H, CH_3, Xanthphos), 1.58 (t, J = 7.1 Hz, 6H, CH_3, dcbq). ^{31}P{^{1}H} NMR (121.5 MHz, $CDCl_3$, 298K): -11.06 (br, 2P, Xantphos), -144.28 (sept, 1P, PF_6, , ^1J(P-F) = 712 Hz).

Photophysical and electrochemical characterization

Steady-state absorption spectra recorded with a Perkin Elmer Lambda 35. Steady-state emission spectra recorded with a Fluoromax-P-spectrometer from HORIBA Jobin Yvon. Cyclic voltammetry and SWV performed with a Methrom μAutolabIII/FRA3, a glassy carbon electrode as working electrode, a silver wire as pseudo-reference electrode and a platinum wire as counter electrode. All spectra were recorded in CH3CN at a concentration of $5 \cdot 10^{-5}$ M with tetrabutylammonium hexafluorophosphate (c=0.1 M) as electrolyte and corrected *vs*. Fc/Fc^+ redox couple. PLQY measurements in powder were performed and referenced against $[Ru(bpy)_3][PF_6]_2$. Lifetimes in powder were measured using nanosecond laser flash photolysis transient absorption measurements, which were carried out with an Nd/YAG laser (third harmonic, 355 nm, 10 mJ) from Brilliant B, Quantel. The optical detection is based on a pulsed (pulser MSP 05 – Müller Elektronik Optik) xenon lamp (XBO 450, Osram), a monochromator (Spectra Pro 2300i, Acton

Research), a fast InGaAs photodiode (Nano 5, Coherent) with 300 MHz amplification, and a 1 GHz digital oscilloscope (WavePro7100, LeCroy). Data was fitted using a biexponential fitting function. Lifetimes and PLQYs in thin film were obtained with an Edinburgh FS5 spectrofluorometer with microsecond lamp and integrating sphere.

Device fabrication and analysis

Double layer LECs were fabricated as follows. ITO coated glass plates were patterned by conventional photolithography (Naranjo Substrates). The substrates were cleaned by using sequential ultrasonic baths, namely in water-soap, water, ethanol, and propan-2-ol solvents. After drying, the substrates were placed in an UV-ozone cleaner (Jetlight 42-220) for 8 min. A 80 nm layer of PEDOT:PSS was doctor-bladed onto the ITO-glass substrate to increase the device preparation yield (400 μm substrate distance and a speed of 10 mm/s). The luminescent layer was entirely prepared with **1**-**3** dissolved in CH_3CN. at a concentration of 20mg/mL or by mixing **3** with CBP in different weight ratios. The active layer was deposited by means of spin coating in a three step process of 800/1200/3000 rpm for 60 s reaching a thickness of 120 nm. These conditions resulted in homogenous thin films with a RMS less than 0.20 nm, having no apparent optical defects. The latter was determined by atomic force microscopy (AFM) in tapping mode on a NanoMan VS AFM (Vecco) and using the profilometer DektakxT (Bruker). Once the active layer was deposited, the samples were transferred into an inert atmosphere glovebox (<0.1 ppm O_2 and H_2O, Anstrong Engineering). Physical vapor deposition of aluminum cathode electrodes (90 nm) was done *via* physical vapor deposition using a shadow mask under high vacuum ($<1x10^{-6}$ mbar) in an Angstrom Covap evaporator integrated into the inert atmosphere glovebox. Time dependence of irradiance, voltage, and current measured by applying constant and/or pulsed voltage and current by monitoring the desired parameters simultaneously by using Avantes spectrophotometer (Avaspec-ULS2048L-USB2) in conjunction with a calibrated integrated sphere Avasphere 30-Irrad and Botest OLT OLED Lifetime-Test System. Electroluminescence spectra were recorded using the above mentioned spectrophotometer. Electrochemical impedance spectroscopic assays (EIS) were carried out with a potentiostat/galvanostat (PGSTAT30, Autolab) equipped with a frequency response analyser module (FRA). Measurements were performed at the applied voltage range from 0 to 5 V. The AC signal amplitude was set to 50 mV, modulated in a frequency range from 10 to 10^6 Hz. The software 'Nova 1.11' was used to obtain the parameters from the equivalent circuit[48,49] following the procedure reported by Brug *et al*.[50] and Hirschorn *et al*.[51]

$$C_{eff} = Q^{(1/\alpha)} R^{(1-\alpha)/\alpha} \quad (1)$$

with C_{eff} is the effective capacitance and R the resistance, Q and α being frequency independent parameters. With this data at hand, the R (active layer) was directly obtained and the relative dielectric constant (ε_r) was calculated by means of equation 2:

$$\varepsilon_r = (C_{eff}\, d)/(\varepsilon_0\, A) \quad (2)$$

where C_{eff} is the capacitance value obtained from the fitting, ε_0 is the permittivity of free space, A is the device area, and d is the thickness of the active layer. The equivalent circuit model for the fittings is shown in the supporting information. With

$$\sigma = d/(R\, A) \quad (3)$$

the effective conductivity was calculated.

RESULTS AND DISCUSSION

Synthesis and characterization

A detailed description of the synthesis and the characterization of the complexes can be found in the Experimental Section. In brief, the syntheses of the Cu(I) iTMCs was carried out following a standard 2-steps/1-pot method in CH_2Cl_2 at room temperature – Figure 1: First, tetrakis-acetonitrile copper(I) reacts with the phosphine ligand, then dcbq is subsequently added. Evaporation of the solvent and addition of diethylether allows the crystallization of the complexes as deep-red solids in good yields. The most relevant feature of the NMR characterization is the broad singlet of the phosphine in the $^{31}P\{^1H\}$ NMR (-2.02 ppm **1**, -10.66 ppm **2**, -11.06 ppm **3**) that, in all cases, integrates 2:1 with respect to the septuplet of the PF_6 anion – Figure S1-3. While complexes **2** and **3** are isolated as pure solids the ^1H NMR spectra of **1** shows that, in solution, the complex is in equilibrium with the homoleptic side products $[Cu(dcbq)_2]^+$ and $Cu(PPh_3)_4]^+$ – Figure S1-3. This type of ligand exchange has been previously reported with copper(I) complexes based on N^N and P^P bidentate ligands,[52] so it is therefore not surprising that such exchange can be also be observed in the particular case of complex **1**, as the absence of chelating diphosphine is surely enhancing the ligand reorganization in solution.

Photophysical characterization

The UV-Vis absorption spectra of complexes **1-3** in CH_2Cl_2 solution are characterized by strong high-energy bands at ~280 nm followed by a less intense band at around 375 nm and a weak band in the green-yellow region– Figure 2. The high-energy absorptions present a ligand-centered (LC)

energy transfer character, representing an intraligand $\pi \rightarrow \pi^*$ transition. The low-energy bands at 370-500 nm are characteristic of the formation of the complexes and responsible of the deep-red color in solution. These bands are attributed to metal-to-ligand (dcbq) charge-transfer transitions (MLCT).[44,53–57] As was mentioned before, the NMR characterization of $[Cu(dcbq)(PPh_3)_2](PF_6)$ **1** in $CDCl_3$ reveals the presence of an equilibrium process of the complex with $[Cu(dcbq)_2]^+$ and $Cu(PPh_3)_4]^+$. In concordance, the UV-Vis absorption spectrum of **1** in CH_2Cl_2 shows an additional absorption band located at *ca*. 577 nm that is attributed to the homoleptic $[Cu(N^N)_2]^+$.

The complexes show intense photoluminescence in fluid and rigid media. Table 1 summarizes the photophysical properties of the complexes and selected examples are shown in Figure 2.

In CH_2Cl_2 solution, the complexes exhibit featureless bands (λ_{max}= 704 **1**, 709 **2**, and 701 **3** nm) that are remarkable blue-shifted in the solid (λ_{max}= 669 **1**, 676 **2**, and 671 **3** nm). This may be attributed to existing J-type aggregates of the compounds in the solid, which typically lead to a hypsochromic shift due to a change in the molecular geometry in the excited state.[10]

The PLQYs (%) in the solid state (0.26 **1** to 0.36 **2** and 0.56 **3**) increase as the P^P moiety becomes more rigid, highlighting the well-known impact of a proper ligand design on preventing a flattening of the complex in the excited emitting state.[44,55,58–63] The excited state decay profiles revealed average lifetimes $<\tau>$ of 0.71, 0.58 and 0.63 µs for **1**, **2** and **3**, respectively. The average radiative rate constants $<k_r>$ increases in line with the PLQY (see Table 1 and Figure S4).

The thin films prepared by spin coating acetonitrile solutions of the corresponding complexes follow the same intensity trend (PLQYs of 0.1% **1**, 1.3% **2**, and 2.3% **3**).

Taking into account the photophysical characterization, complex $[Cu(dcbq)(Xantphos)](PF_6)$ **3** clearly overcomes its brothers as the best emitter candidate for red lighting devices.

Electrochemical characterization

Considering the intrinsic device mechanism – *vide infra* - the emitter must be stable towards oxidation and reduction. We therefore studied the redox-features of **1**-**3** with cyclovoltammetric (CV) and square wave voltammetry (SWV) assays in acetonitrile (CH_3CN) – Table 1 and Figure S5 and S6. All compounds show a *quasi*-reversible redox behavior, with a small shift of the oxidation potential in the row **3** < **2** < **1** towards lower potentials going from 0.91 **3**, 0.87 **2**, 0.83 **1** V *vs*. Fc/Fc^+, what is in line with the rigidity of the P^P ligand Xantphos > POP > PPh_3. This is, indeed, supported by a linear trend associated to the highest occupied molecular orbital (HOMO), which is usually located across the Cu(I) central atom and the P^P ligand.

The three complexes present a first reduction wave at -1.3 V *vs*. Fc/Fc^+, which is ascribed to the N^N ligand (dcbq), upon which the LUMO is presumably located (see Table 1). Additionally, the complexes present a second reduction wave at -1.51, -1.70 and -1.76 V *vs*. Fc/Fc^+ for **1**, **2**, and **3**, respectively. This second reduction is assigned to the P^P ligand, which presents additional accessibility for electronic reduction. In order to identify the level of *quasi*-reversibility of the series, we further corroborated the ratio of the first oxidation and reduction peak, respectively, of the SWV assays by integrating the peak derived in forward and reverse scanning direction, *i.e*., upon scanning from the cathodic to the anodic direction and *vice versa* – Figure S6. The obtained ratio increases linearly within the series, *i.e*., from **1** to **3**, for both the oxidation and reduction processes. Thus, the stability towards hole transport under device operation in the compounds points to a clear trend that goes hand-in-hand with the rigidity of the present P^P ligand – Figure 1. Once again, complex [Cu(dcbq)(Xantphos)](PF_6) **3** shows the best electrochemical behavior for LECs.

Solid state studies

It is essential to have a homogeneous and defect-free active layer in a device architecture. We prepared layers comprising the respective compound on a glass/ITO/poly(3,4-ethylenedioxythiophene) polystyrene sulfonate (PEDOT:PSS) (90 nm)/active layer (120 nm) – see experimental section for details. The morphology of the layers thus prepared were studied by atomic force microscopy (AFM) and the electronic transport measured by electrochemical impedance spectroscopy (EIS). With the three complexes **1**-**3**, we were able to prepare homogeneous layers with an active layer thickness of 120 nm and very low root mean square (RMS) roughness values of around 0.2 nm in a 5 μm^2 sample area. This accounts for a similar layer morphology, *e.g*., sample images from layers prepared **1**-**3** – Figure 3.

When getting an insight into the electrical behavior of the layers, we found clear indications that the integrity of complex **1** was lost. For this reason, we focus on EIS analysis of layers prepared with **2** and **3**, putting special emphasis on comparing freshly *vs*. after pre-biasing the layers. The fresh samples show similar trends in resistance at low voltages, *i.e*., < 1.5 V, and similar ionic conductivity of 4.1×10^{-9} S/m and 3.6×10^{-9} S/m for **2** and **3**, respectively. Devices made from **3** show a quicker electrical double layers (EDL) formation than devices made from **2**, as it is shown by the steeper slope of the resistance versus applied voltage curve at voltage lower than the

injection voltage (V_{inj}). This leads to decreased resistance at the same applied voltage (*e.g.* 2.3 × 10^5 Ω *vs* 6.5 × 10^4 Ω at 2.5 V) – Table S1 and Figure 4.

This is in perfect agreement with the dielectric constant (ε_r), which is almost twice in **3** (9.8 **3** *vs* 5.3 **2**), despite both show the same ionic conductivity. There is a direct relationship between the rearrangement of a molecule and its dipole moment and ε_r, so it can be said that **3** rearranges faster upon applying an electric field, and, therefore, it is more suitable for lighting devices.[64]

After pre-biasing both layers their resistance decrease, what is logical given that the EDLs are formed in the pre-biasing. When comparing pre-biased with fresh devices, those prepared from **3** show higher ionic conductivity 2.74 × 10^{-6} Ω and higher ε_r 12.6, while layers prepared from **2** show more resistance (1.96 × 10^8 vs 1.1 × 10^{10} Ω at 0 V). This highlights the irreversible formation of new species upon applied voltage what can result in lower stability of the devices.

Electroluminescent behavior of red Cu(I)-iTMCs in LECs

LECs implies that the emitter is responsible of charge injection, transport and emission processes.[31,65,66] In short, mobile ions are at first randomly distributed throughout the entire active layer. After biasing the device, the ions move towards the respective electrodes, forming EDLs at the electrode/active layer interfaces. Thus, ohmic contacts form, leading to a heavy doping of the active layer and to an efficient increase in current and electroluminescence (EL). This unique feature allows the use of electrode materials fairly independent to their work functions response.[67] By further biasing the device, injection of electrons (holes) at the cathode (anode) occurs and leads to n- and p-doped regions, which grow towards each other, creating an intrinsic region in between, where holes and electrons recombine under emission of light. As in iTMCs the cation is mostly bulkier than the small counter-anion (*e.g.* PF_6), the charge migration is unfavorably balanced, leading to a shift of the emission zone away from the center as shown in planar devices.[68] In this context, the introduction of supporting electrolytes and/or the use of double-layer architectures have proved to be effective strategies to enhance the device performances. [22,38,44,45]

As discussed before, taking all of the aforementioned into account, the sequence of the best suited emitter in this family of $[Cu(N^N)(P^P)]^+$ in terms of stability and efficiency is estimated to decrease from **3** to **1**. Thereby, the key figures-of-merit preferentially ruling the device performance are considered to be (i) the PLQY, (ii) the redox stability, (iii) the morphology, and (iv) the stable electronic device behavior.

To shed light on this, we prepared LEC devices from compounds **1**-**3** in a sandwich-like device architecture based on a Al metal cathode and an active layer comprising **1**-**3** on top of a glass/ITO anode coated with a PEDOT:PSS layer – see experimental section for details. During luminance-current-voltage (LIV) assays in the form of 5 cycles of 0-18 V voltage scan at 300 mV/s, the current density holds constant for devices with **3,** while devices with **1** and **2** feature an enhancement up to the 4th scan cycle. Going hand-in hand, the luminescence increases with the number of cycles for devices with **2** and **3**, while devices with **1** show a decrease upon injection over time. This can be ascribed to the different level of electrochemical reversibility of the complexes, but it must be mentioned again that layers made of **1** also contain impurities that surely affect the properties of the layer in great extent. The devices show stable deep-red emission with x/y CIE 0.52/0.33 (**1**), and 0.66/0.32 (**2** and **3**) and the absolute highest value of irradiance follows the PLQYs in thin films; **1** < **2** < **3**. In particular, the maximum light output of the devices increases from 0.89 **1** to 29.2 **2** to 33.0 **3** μW/cm^2 –Figures 5 and S7. Devices with **3** show the lowest injection voltage of 2.5 V to note light response, as expected from the easier formation of the EDLs.

With this data at hand, we turned to lifetime measurements of the devices – Figures 5 and S8. We therefore applied a driving mode based on an average current of either 15 or 20 mA in a pulsed current scheme at a standard block wave of 1 kHz and a duty cycle of 50%–Table 2. The pulsed driving scheme led to best performing LECs with fast turn-on times and long-time stabilities.[15,31] On one hand, for all the three complexes, the voltage profile follows the typical LEC behavior, *i.e.,* the rapid drop of the initial average voltage due to the EDL formation and of the doping process in the active layer, thus reducing the voltage until reaching steady state conditions, whereby the voltage reaches a stable plateau.

As was expected, the maximum irradiance and stability, given by $t_{1/2}$, of devices made from **3** overcomes those of **2** and **1** (97.9 μW/cm^2, 20.9 h **3**; 41.5 μW/cm^2, 6.5 h **2**; 0.77 μW/cm^2, 1.7·10^{-3} h **1**). These data highlights the superior performances of **3** devices– Figures 5 and S7.

The analysis of the total emitted energy, obtained by taking the time needed to reach one fifth of the maximum luminance as the upper limit, allows a clear stability comparison of devices showing different luminance levels as indicated by Bard and co-workers.[69] Once again, **3** shows enhanced irradiance as well as stability –Table 2. This is supported by EIS assays, as **1** and **2** present an inefficient charge mobility shortly after pre-biasing the device, which generates charge unbalance upon applied voltage and a fast drop of the irradiance. In line with the LIV-studies, the total emitted

energy of **3** devices increases up to eight orders of magnitude compared to **1**, resulting in stable deep-red-emitting LECs with broad shape EL and CIE 1931 coordinates of x/y of 0.66 / 0.32 and lifetimes of more than 20 h – Figures 5, S8 and Table 2.

Next, we elucidated the effect of a supporting electrolyte introduced to the active layer in order to enhance the device performance. Therefore, we used the ionic liquid (IL) 1-ethyl-3-methylimidazolium hexafluorophosphate, EMIM PF_6, mixed in a molar ratio of 4:1 with compounds **1**-**3**, and studied the effect on the device performance. One can usually expect to enhance the overall device performance by effectively assisting the EDL formation and, thus, the doping process, leading to a faster and higher light output, *vide supra.* As reported in many studies, the mixtures of ILs and Cu-iTMCs are prone to crystallization upon film forming. [37,44] Hence, we firstly studied the layer quality for the device architecture ITO / PEDOT:PSS / Cu(I)-iTMC:IL in a molar ratio of 4:1. Contrary to what has been observed in the literature,[15,38,70] the blended ones showed no significant difference in layer quality featuring a thickness of 120 nm and an active layer RMS roughness of <0.2 nm– Figure 3. Additionally, the PLQYs values raises to 0.2%, 2.5% and 6.1% for the 4:1 mixture and to 0.2%, 3.0% and 6.8% for the 1:1 ratio.

Devices with the intermixed IL showed similar EL and CIE coordinates to the pristine compounds – Table S2. In the blended devices, **1** shows light output at 20 mA, and its total emitted energy, is in the same range than for the pristine device (3.7×10^{-5} J *vs* 5.0×10^{-5} J) for pristine and **1**:IL in ratio 4:1, respectively. This is stemming most likely from the instability of the complex in solution and the presence of different species in thin films. For this reason, we further focused on compounds **2** and **3**, as these turned out to be the most promising compounds as emitters in devices, *vide supra*. The higher amount of mobile ions in the active layer leads to overall lower lifetimes- *e.g.* from 20.9 h for **3** pristine to a few minutes for **3**:IL –Figure 5 and S9. Taking into account that the PLQYs of the layers with the IL are higher than without it but the morphology, as proved by AFM, are similar, the reason underlying the reduced lifetime in the IL containing devices are ascribed to an excessive growth of the n- and p- doped regions. Thus, the supporting electrolyte has a much higher impact on the total emitted energy of the device from both **2** and **3** and reveals a drop of the overall light output by drastically shortening the lifetime.

The EIS characteristics shed light on this behavior– Figure 4 and Table S2. We performed EIS assay of devices from compound **3** with two different blending ratio of IL, *i.e.*, 4:1 and 1:1 – Figure S10. As expected, samples comprising ILs showed a higher ionic conductivity than the pristine

ones, owing to the higher concentration of mobile ions provided by the electrolyte. This led to one order of magnitude decrease in resistance at 0 V -Figure 4 and S11. Similarly, the dielectric constant ε reduces from 9.79, to 8.54 and to 7.53 going from pure **3** to increasing amounts of EMIM PF_6– Table S1. A ratio 4:1 of IL leads to an overall drop in the resistance during the entire measurement. When a 1:1 ratio is employed, low resistance and a quick EDL formation in the fresh devices is noted but an overall increase in the resistance is observed when passing from fresh to biased devices (*e.g.* 2.36×10^6 *vs* 9.88×10^5 for fresh and biased devices respectively at 0 V), indicating the presence of irreversible oxidation or reduction processes. We conclude that the introduction of additional mobile ions creates an excessive charge density, leading to a fast deterioration of the device properties– Table S1. This explains the drop in lifetime and light output and is summarized by the total emitted energy, which decreases for a driving mode of 15 mA from 135.4 J, to 5.1 J, and to 7.0×10^{-3} for pristine, 4:1, and 1:1 blend, respectively. Increasing the amount of ionic liquid, therefore, reduces the overall figures-of-merit expressed in a lower stability and light output.– Figure S9.

Taking all of the aforementioned into account, it is safe to conclude that devices prepared from this series of Cu(I)-iTMCs **1**-**3** can be successful implemented in lighting devices to create deep-red LECs. Here, the addition of IL as supporting electrolyte gave no enhancement of the device figures-of-merit and the best-suited compound for LECs turned out to be compound **3**.

*White-emitting LECs with **3***

Complex **3** shows the most efficient deep-red electroluminescence and the ideal candidate for act as guest with the HTM CBP, which is a high bandgap material with a blue PL and EL response that fit the absorption of **3**. A good energy transfer in a traditional host-guest system is predictable, given by the HOMO-LUMO energy levels of both molecules–Figure 6.

The commonly used HTM can be implemented in the device by mixing it with the emitter in the active layer, resulting in a device architecture ITO/PEDOT:PSS/**3**:CBP/Al –see experimental section for details. By changing the blending ratio in a range 1-30 wt% of **3**, the EL response can be tuned to obtain a white light output. With 1% wt of **3**, the EL shows only the CBP response at around 390 and 490 nm but as the amount of **3** increases the energy transfer from CBP to **3** becomes more efficient – Figure 6. A 15% wt is enough to generate white EL response with CIE 1931 coordinates of x/y of 0.31/0.32 and CRI of 92. This EL response is stable over the lifetime showing a moderate luminance of 4 cd/m^2 and efficiency of 0.001 cd/A at 25 mA – Figure 6. The luminance

value is moderate; however, this value has to be put into context, considering that CBP:TMPE:LiOTf devices only produces a luminance of 5 cd/m^2 when running at the driving current of 25 mA– Figure S10. Noteworthy, a 30% wt of **3** resulted in slightly lower luminances compared to pure **3** devices when measured at 15 mA (79 μW/cm^2), but with an outstanding stability of 170 h– Figure S14. In this case, the energy transfer from CBP to **3** is complete, leading to an emission with λ_{max} 670 nm that is stable over time and is coming entirely from **3**– Figure S14. Overall, these examples shows the potential of effectively mixing [Cu(dcbq)(Xantphos)](PF$_6$) **3** with other emissive materials to build highly stable deep-red or white-emitting LECs and paves the way for low-cost white lighting sources from single layer EL devices.

CONCLUSIONS

Firstly, a novel family of [Cu(dcbq)(P^P)](PF$_6$) complexes (P^P = 2 PPh$_3$ **1**, POP **2** or Xantphos **3**) has been synthetized and characterized and the photophysical and electrochemical properties studied. We found that increasing the rigidity of the diphosphine provides enhanced electrochemical stability, reversibility and higher PLQY. The same trend is reflected in the stability and light output of **1**-**3** based LEC devices. In particular, the complex bearing Xantphos as P^P ligand showed a promising light quality, *i.e.*, stable deep-red EL spectrum centered at around 675 nm, x/y CIE of 0.66/0.32, irradiance of ~ 100 μW/cm^2 and stability of 21 h.

Optimization with the IL EMIMPF$_6$ showed no significant difference in layer quality as corroborated by AFM assays, and slightly higher PLQYs. However, the devices showed decreased stability and total emitted energy with IL as compared to the pristine samples. By EIS, we found that the reason for this is that the increased ionic conductivity leads to an excessive charge density in the layer.

Secondly, the better performing compound **3** was used in a host-guest system with the HTM CBP to achieve proof-of-concept white emitting LECs featuring CIE 1931 coordinates of x/y = 0.31 / 0.32 and a high CRI of 92.

Last but not less the use of a ratio 70:30 CBP:**3** allowed us to prepare deep-red emissive LECs with λ_{max} 672 nm and slightly reduced irradiances of 79 μW/cm^2 compared to pristine **3**. However, this strategy provides outstanding improved stability of 170 h.

Overall, this work provides the first example of deep-red and white emitting devices based on Cu(I) complexes in LECs, bridging the gap to explore emitters covering the whole visible range for future applications.

FIGURES

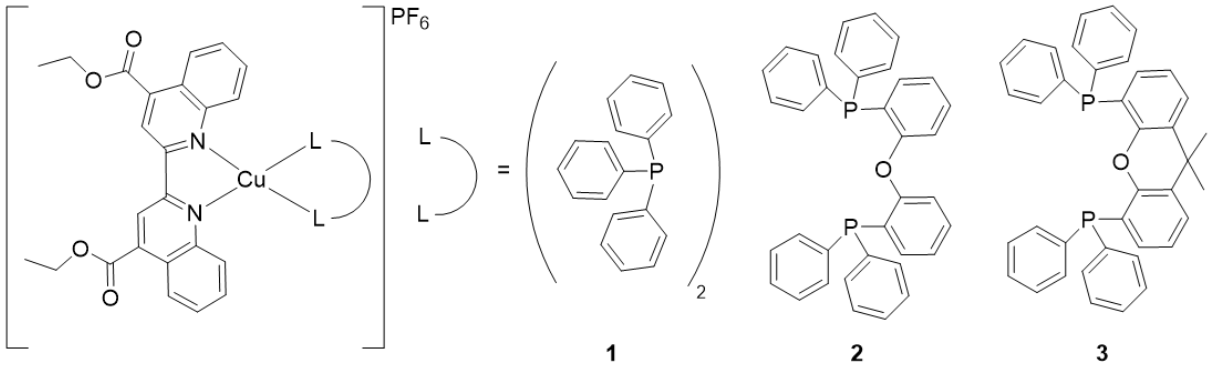

Figure 1. Chemical structures of complexes **1**-**3**.

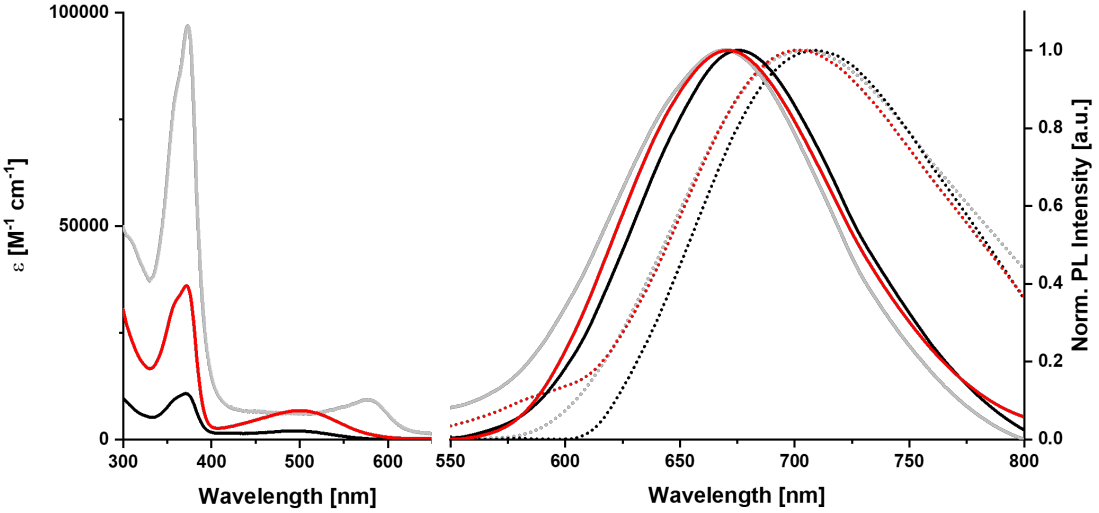

Figure 2. Left: Absorption spectra of **1** (grey line), **2** (black line) and **3** (red line) at a concentration of 10^{-4} M. Right: Emission in DCM (dotted lines) at excitation wavelength of 490 nm (bottom left) recorded in DCM solution and powder PL (solid lines) at excitation at 420 nm of complexes **1** (grey lines), **2** (black lines) and **3** (red lines).

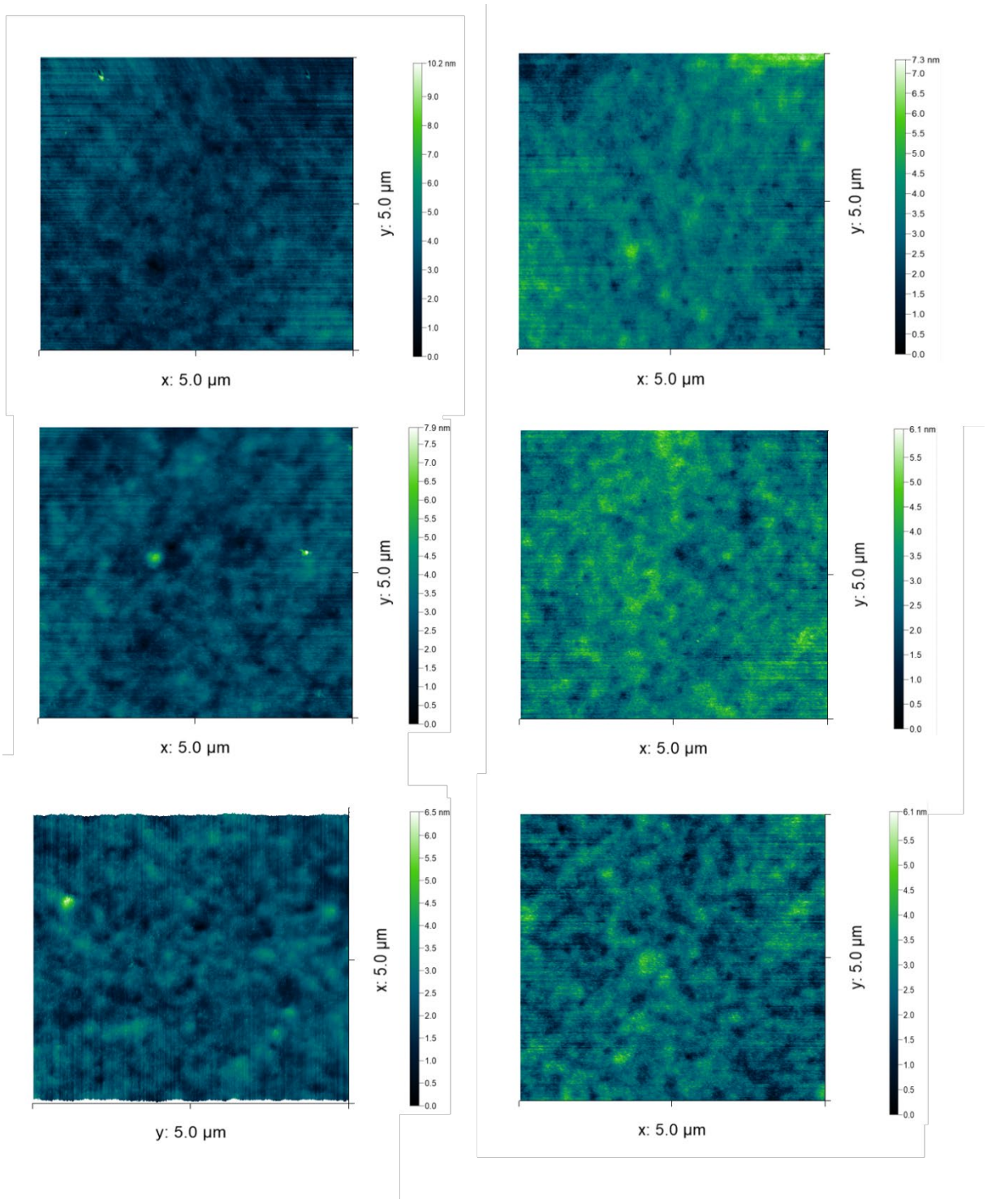

Figure 3. AFM microscopy study: a) layer prepared from pristine **1-3** (top, centre and bottom left, respectively) and **1-3**:IL in 4:1 molar ratio (top, centre and bottom right, respectively).

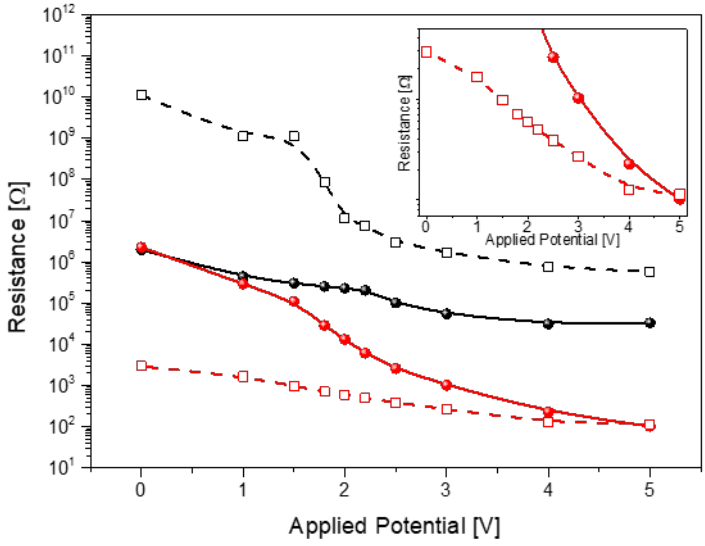

Figure 4. Resistance change derived from EIS data in a solid-state configuration for pristine **2** (black) and **3** (red) in fresh (solid line) and pre-biased condition (dashed line). Inset shows the detailed zoom-in for compound **3**.

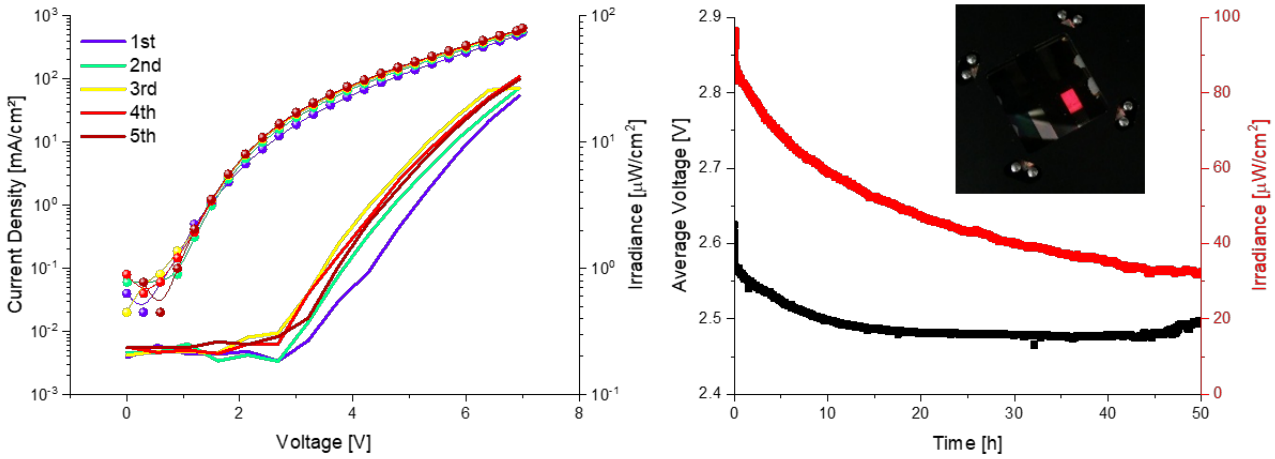

Figure 5. LEC device performance of compound **3**. Repetitive current-voltage sweeps and light output of a device prepared from pristine **3** in a voltage range of 0-7 V reached with a step potential of 300 mV/s (left) and lifetime measurement in pulsed galvanostatic driving scheme at an average current of 15 mA (right, inset shows a picture of a device under operation).

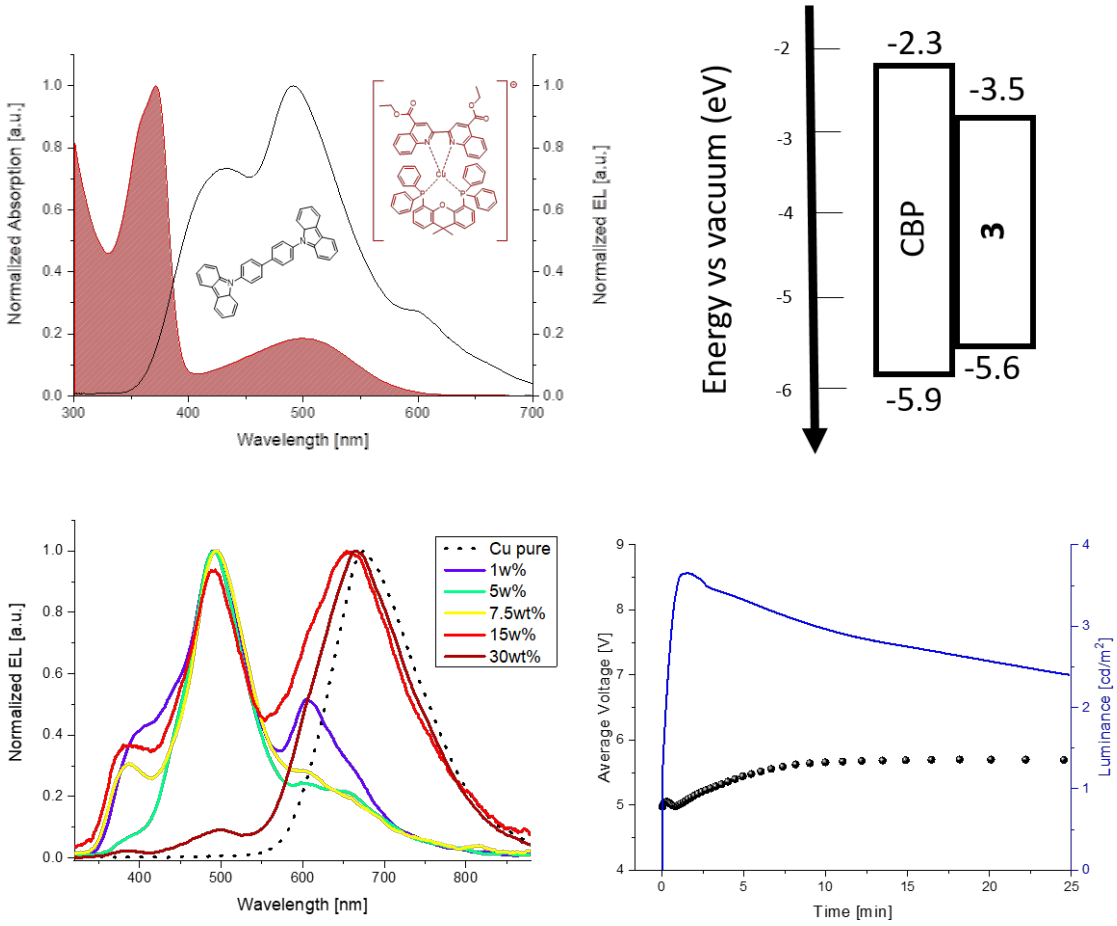

Figure 6. Top: Normalized absorption of **3** (red) showing an overlap to the EL (black) of CBP (left), energy levels of CBP and **3** as derived from the CV data with the formula $E_{HOMO/LUMO}$ = e(VCp/Cp^+) + 4.8 eV (right) and EL response of different blending ratios in wt% of **3** with CBP (right). Bottom: EL response of different blending ratios in wt% of **3** with CBP (left), and lifetime measurement at pulsed galvanostatic driving scheme at an average current of 25 mA of a white device containing compound **3** at 15 wt% blended in CBP (left) and the corresponding CIE 1913 coordinates of the single components and the white device (right).

TABLES.

Table 1. Photophysical characterization of **1-3**.

Compound	Molar absorptivity[a] ε [10^4·L·mol^{-1}·cm^{-1}]) at λ_{max} (nm)	PL[b] λ_{em} [nm]	λ_{solid}[c] [nm]	Cyclovoltammetry[d] E_{ox} [V]	E_{red} [V]	PLQY[e] ϕ_{PL} [%]	PLQY[f] ϕ_{PL} [%]	Average data[g] $<\tau>^g$ [μs]	$<\tau>^h$	lifetime $<k_r>$ [10^9·s^{-1}]	$<k_{nr}>$ [10^{12}·s^{-1}]
1	24.1 (277), 9.69 (373), 0.93 (577)	704	669	0.91	-1.26	0.26	0.1	0.707	0.88	3.65	1.41
2	13.3 (277), 1.08 (371), 0.21 (497)	709	676	0.87	-1.30	0.35	1.3	0.582	1.96	6.06	1.71
3	12.4 (276), 3.61 (372), 0.68 (501)	701	671	0.83	-1.26	0.56	2.3	0.627	1.85	8.87	1.59

[a] in CH_2Cl_2, concentration 10^{-5} mol·L^{-1}. [b] in CH_2Cl_2, concentration 10^{-4} mol·L^{-1} at excitation of 490 nm. [c] in powder at excitation of 420 nm. [d] first reduction and oxidation peak *vs*. Fc/Fc$^+$. [e] in powder *vs*. $[Ru(bpy)_3][PF_6]_2$ reference (error ±10%). [f] in thin film. [g] excited state-lifetimes measured in powder upon excitation at 355 nm. [h]. excited state-lifetimes measured in thin film upon excitation at 355 nm.

Table 2. Lifetime data of **1-3** devices.

Device	Current Density [mA/cm^2]	Average Current [mA]	Irradiance [μW/cm^2]	$t_{1/2}$[a] [h]	$t_{1/5}$[b] [h]	E_{tot}[c] [J]	$\lambda_{max, EL}$ [nm]	CIE 1931 coordinates x/y
1	133.1	20	0.77	1.4E-3	3.1E-3	3.74E-05	670	0.524 / 0.334
	100.4	15	0.90	1.7E-3	4.7E-3	7.15E-05		
2	132.1	20	50.1	1.3	5.7	5.50E+01	672	0.661 / 0.323
	99.85	15	41.1	6.5	20.0	1.39E+02		
3	133.35	20	129.8	3.12	24.8	5.46E+02	675	0.660 / 0.320
	99.92	15	97.9	20.9	81.2	1.34E+03		

[a] time to reach 50% of the initial irradiance. [b] time to reach 20% of the initial irradiance. [c] total emitted energy.

ASSOCIATED CONTENT

^{1}H-NMR and ^{13}C-NMR spectra of **1-3**, excited state lifetimes, cyclic and square-wave voltammetry, device performances, and Nyquist plots are avalaible in the **Supporting Information**.

AUTHOR INFORMATION

Corresponding Author

ruben.costa@imdea.org

Author Contributions

The manuscript was written through contributions of all authors. All authors have given approval to the final version of the manuscript.

Funding Sources

E.F., J.F-C. and R.D.C. acknowledge the program "Ayudas para la atracción de talento investigador – Modalidad 1 of the Consejería de Educación, Juventud y Deporte – Comunidad de Madrid with the reference number 2016-T1/IND-1463". R. D. C. acknowledges Spanish MINECO for the Ramón y Cajal program (RYC-2016-20891), the Europa Excelencia program (ERC2019-092825), and the 2018 Leonardo Grant for Researchers and Cultural Creators from BBVA Foundation.
R.D.C and M.D.W. acknowledge funding by the 'Fonds der Chemischen Industrie' (FCI) in the Liebig grant framework and the Cluster of Excellence 'Engineering of Advanced Materials' (EAM).
ACKNOWLEDGMENT

The authors are thankful to Y. Lao, X. Zhang, E. Baranoff, for the synthesis work.

REFERENCES

(1) Humphreys, C. J. USE Solid-State Lighting. *MRS Bull.* **2008**, *33* (04), 459–471.

(2) Volz, D.; Wallesch, M.; Fléchon, C.; Danz, M.; Verma, A.; Navarro, J. M.; Zink, D. M.; Bräse, S.; Baumann, T. From Iridium and Platinum to Copper and Carbon: New Avenues for More Sustainability in Organic Light-Emitting Diodes. *Green Chem.* **2015**, *17* (4), 1988–2011.

(3) Czerwieniec, R.; Yersin, H. Diversity of Copper(I) Complexes Showing Thermally Activated Delayed Fluorescence: Basic Photophysical Analysis. *Inorg. Chem.* **2015**, *54* (9), 4322–4327.

(4) Tao, Y.; Yuan, K.; Chen, T.; Xu, P.; Li, H.; Chen, R.; Zheng, C.; Zhang, L.; Huang, W. Thermally Activated Delayed Fluorescence Materials towards the Breakthrough of Organoelectronics. *Adv. Mater.* **2014**, *26* (47), 7931–7958.

(5) Dumur, F. Recent Advances in Organic Light-Emitting Devices Comprising Copper Complexes: A Realistic Approach for Low-Cost and Highly Emissive Devices? *Org. Electron. physics, Mater. Appl.* **2015**, *21*, 27–39.

(6) Igawa, S.; Hashimoto, M.; Kawata, I.; Yashima, M.; Hoshino, M.; Osawa, M. Highly Efficient Green Organic Light-Emitting Diodes Containing Luminescent Tetrahedral Copper(<scp>i</Scp>) Complexes. *J. Mater. Chem. C* **2013**, *1* (3), 542–551.

(7) Tsuge, K.; Chishina, Y.; Hashiguchi, H.; Sasaki, Y.; Kato, M.; Ishizaka, S.; Kitamura, N. Luminescent Copper(I) Complexes with Halogenido-Bridged Dimeric Core. *Coord. Chem. Rev.* **2016**, *306*, 636–651.

(8) Cariati, E.; Lucenti, E.; Botta, C.; Giovanella, U.; Marinotto, D.; Righetto, S. Cu(I) Hybrid Inorganic-Organic Materials with Intriguing Stimuli Responsive and Optoelectronic

Properties. *Coord. Chem. Rev.* **2016**, *306*, 566–614.

(9) Chihaya, A. Third-Generation Organic Electroluminescence Materials. *Jpn. J. Appl. Phys.* **2014**, *53* (6), 60101.

(10) Yersin, H.; Rausch, A. F.; Czerwieniec, R.; Hofbeck, T.; Fischer, T. The Triplet State of Organo-Transition Metal Compounds. Triplet Harvesting and Singlet Harvesting for Efficient OLEDs. *Coord. Chem. Rev.* **2011**, *255* (21–22), 2622–2652.

(11) Cheng, G.; So, G. K.-M.; To, W.-P.; Chen, Y.; Kwok, C.-C.; Ma, C.; Guan, X.; Chang, X.; Kwok, W.-M.; Che, C.-M. Luminescent Zinc(Ii) and Copper(i) Complexes for High-Performance Solution-Processed Monochromic and White Organic Light-Emitting Devices. *Chem. Sci.* **2015**, *6* (8), 4623–4635.

(12) Qibing, P.; Gang, Y.; Chi, Z.; Yang, Y.; Alan J., H. Polymer Light-Emiting Electrochemical Cells. *Science (80-.).* **1995**, *269* (8), 1086–1088.

(13) Fresta, E.; Costa, R. D. Beyond Traditional Light-Emitting Electrochemical Cells-a Review of New Device Designs and Emitters. *J. Mater. Chem. C* **2017**, *5* (23), 5643–5675.

(14) Costa, R. D. *Light-Emitting Electrochemical Cells. Concepts, Advances and Challenges.*, 1st ed.; Springer International Publishing: Basel, 2017.

(15) Costa, R. D.; Ortí, E.; Bolink, H. J.; Monti, F.; Accorsi, G.; Armaroli, N. Luminescent Ionic Transition-Metal Complexes for Light-Emitting Electrochemical Cells. *Angew. Chemie - Int. Ed.* **2012**, *51* (33), 8178–8211.

(16) Asadpoordarvish, A.; Sandström, A.; Larsen, C.; Bollström, R.; Toivakka, M.; Österbacka,

R.; Edman, L. Light-Emitting Paper. *Adv. Funct. Mater.* **2015**, *25* (21), 3238–3245.

(17) Sandström, A.; Edman, L. Towards High-Throughput Coating and Printing of Light-Emitting Electrochemical Cells: A Review and Cost Analysis of Current and Future Methods. *Energy Technol.* **2015**, *3* (4), 329–339.

(18) Sandstroem, A.; Asadpoordarvish, A.; Enevold, J.; Edman, L. Spraying Light: Ambient-Air Fabrication of Large-Area Emissive Devices on Complex-Shaped Surfaces. *Adv. Mater.* **2014**, *26* (29), 4975–4980.

(19) Rudmann, H.; Shimada, S.; Rubner, M. F. Solid-State Light-Emitting Devices Based on the Tris-Chelated Devices Based on Derivatives of the Tris (2 , 2 ′ -Bipyridyl) Ruthenium (II) Complex. *J. Am. Chem. Soc.* **2002**, *124* (Ii), 4918–4921.

(20) Flamigni, L.; Barbieri, A.; Sabatini, C.; Ventura, B.; Barigelletti, F. Photochemistry and Photophysics of Coordination Compounds: Iridium BT - Photochemistry and Photophysics of Coordination Compounds II. *Top. Curr. Chem.* **2007**, *281*, 143–203.

(21) Hu, T.; He, L.; Duan, L.; Qiu, Y. Solid-State Light-Emitting Electrochemical Cells Based on Ionic Iridium(Iii) Complexes. *J. Mater. Chem.* **2012**, *22* (10), 4206–4215.

(22) Tordera, D.; Meier, S.; Lenes, M.; Costa, R. D.; Ortí, E.; Sarfert, W.; Bolink, H. J. Simple, Fast, Bright, and Stable Light Sources. *Adv. Mater.* **2012**, *24* (7), 897–900.

(23) Martínez-Alonso, M.; Cerdá, J.; Momblona, C.; Pertegás, A.; Junquera-Hernández, J. M.; Heras, A.; Rodríguez, A. M.; Espino, G.; Bolink, H.; Ortí, E. Highly Stable and Efficient Light-Emitting Electrochemical Cells Based on Cationic Iridium Complexes Bearing

Arylazole Ancillary Ligands. *Inorg. Chem.* **2017**, *56* (17), 10298–10310.

(24) He, L.; Duan, L.; Qiao, J.; Wang, R.; Wei, P.; Wang, L.; Qiu, Y. Blue-Emitting Cationic Iridium Complexes with 2-(1H-Pyrazol-1-Yl)Pyridine as the Ancillary Ligand for Efficient Light-Emitting Electrochemical Cells. *Adv. Funct. Mater.* **2008**, *18* (14), 2123–2131.

(25) Costa, R. D.; Ortì, E.; Bolink, H. J.; Graber, S.; Housecroft, C. E.; Constable, E. C. Efficient and Long-Living Light-Emitting Electrochemical Cells. *Adv. Funct. Mater.* **2010**, *20* (9), 1511–1520.

(26) Housecroft, C. E.; Constable, E. C. Over the LEC Rainbow: Colour and Stability Tuning of Cyclometallated Iridium(III) Complexes in Light-Emitting Electrochemical Cells. *Coord. Chem. Rev.* **2017**, *350*, 155–177.

(27) Henwood, A. F.; Zysman-Colman, E. Luminescent Iridium Complexes Used in Light-Emitting Electrochemical Cells (LEECs). *Top. Curr. Chem.* **2016**, *374* (4), 36.

(28) Emsley, J. *Nature's Building Blocks : An A-Z Guide to the Elements*; Emsley, J., Ed.; Oxford University Press, 2011.

(29) McMillin, D. R.; Buckner, M. T. Photoluminescence From Copper (I) Complexes With Low -Lying Metal-to-Ligand Charge Transfer Excited States. *J.C.S Chem. Comm.* **1978**, *29*, 759–761.

(30) Balzani, C.; Campagna, S.; Armaroli, N.; Accorsi, G.; Cardinali, F.; Listorti, A. Photochemistry and Photophysics of Coordination Compounds. **2007**, *281*, 143–203.

(31) Meier, S. B.; Tordera, D.; Pertegás, A.; Roldán-Carmona, C.; Ortí, E.; Bolink, H. J. Light-

Emitting Electrochemical Cells: Recent Progress and Future Prospects. *Mater. Today* **2014**, *17* (5), 217–223.

(32) Henwood, A. F.; Zysman-Colman, E. Luminescent Iridium Complexes Used in Light-Emitting Electrochemical Cells (LEECs). *Top. Curr. Chem.* **2016**, *374* (4), 36.

(33) Weber, M. D.; Adam, M.; Tykwinski, R. R.; Costa, R. D. Controlling the Chromaticity of Small-Molecule Light-Emitting Electrochemical Cells Based on TIPS-Pentacene. *Adv. Funct. Mater.* **2015**, *25* (31), 5066–5074.

(34) Weber, M. D.; Wittmann, J. E.; Burger, A.; Malcioglu, O. B.; Segarra-Martinez, J.; Hirsch, A.; Coto, P. B.; Bockstedte, M.; Costa, R. D. From White to Red: Electric-Field Dependent Chromaticity of Light-Emitting Electrochemical Cells Based on Archetypal Porphyrins. *Adv. Funct. Mater.* **2016**, *26* (37), 6737–6750.

(35) Tang, S.; Pan, J.; Buchholz, H. a; Edman, L. White Light from a Single-Emitter Light-Emitting Electrochemical Cell. *J. Am. Chem. Soc.* **2013**, *135*, 3647–3652.

(36) Weber, M. D.; Garino, C.; Volpi, G.; Casamassa, E.; Milanesio, M.; Barolo, C.; Costa, R. D. Origin of a Counterintuitive Yellow Light-Emitting Electrochemical Cell Based on a Blue-Emitting Heteroleptic Copper(I) Complex. *Dalt. Trans.* **2016**, *45* (21), 8984–8993.

(37) Elie, M.; Sguerra, F.; Di Meo, F.; Weber, M. D.; Marion, R.; Grimault, A.; Lohier, J.-F.; Stallivieri, A.; Brosseau, A.; Pansu, R. B.; et al. Designing NHC–Copper(I) Dipyridylamine Complexes for Blue Light-Emitting Electrochemical Cells. *ACS Appl. Mater. Interfaces* **2016**, *8* (23), 14678–14691.

(38) Weber, M. D.; Fresta, E.; Elie, M.; Miehlich, M. E.; Renaud, J.-L.; Meyer, K.; Gaillard, S.; Costa, R. D. Rationalizing Fabrication and Design Toward Highly Efficient and Stable Blue Light-Emitting Electrochemical Cells Based on NHC Copper(I) Complexes. *Adv. Funct. Mater.* **2018**, *28* (17), 1707423.

(39) Elie, M.; Weber, M. D.; Di Meo, F.; Sguerra, F.; Lohier, J.-F.; Pansu, R. B.; Renaud, J.-L.; Hamel, M.; Linares, M.; Costa, R. D.; et al. Role of the Bridging Group in Bis-Pyridyl Ligands: Enhancing Both Photo- and Electro-Luminescent Features of Cationic (IPr)Cu(I) Complexes. *Chem. - A Eur. J.* **2017**, *23* (64), 16328–16337.

(40) Zhang, Q.; Zhou, Q.; Cheng, Y.; Wang, L.; Ma, D.; Jing, X.; Wang, F. Highly Efficient Electroluminescence from Green-Light-Emitting Electrochemical Cells Based on CuI Complexes. *Adv. Funct. Mater.* **2006**, *16* (9), 1203–1208.

(41) Keller, S.; Brunner, F.; Junquera-Hernández, J. M.; Pertegás, A.; La-Placa, M.-G.; Prescimone, A.; Constable, E. C.; Bolink, H. J.; Ortí, E.; Housecroft, C. E. CF 3 Substitution of [Cu(P^P)(Bpy)][PF 6] Complexes: Effects on Photophysical Properties and Light-Emitting Electrochemical Cell Performance. *Chempluschem* **2018**, *83* (4), 217–223.

(42) Keller, S.; Constable, E. C.; Housecroft, C. E.; Neuburger, M.; Prescimone, A.; Longo, G.; Pertegás, A.; Sessolo, M.; Bolink, H. J. [Cu(Bpy)(P^P)] + Containing Light-Emitting Electrochemical Cells: Improving Performance through Simple Substitution. *Dalt. Trans.* **2014**, *43* (44), 16593–16596.

(43) Brunner, F.; Martínez-Sarti, L.; Keller, S.; Pertegás, A.; Prescimone, A.; Constable, E. C.; Bolink, H. J.; Housecroft, C. E. Peripheral Halo-Functionalization in [Cu(N^N)(P^P)](+)

Emitters: Influence on the Performances of Light-Emitting Electrochemical Cells. *Dalt. Trans.* **2016**, *45* (38), 15180–15192.

(44) Costa, R. D.; Tordera, D.; Ortí, E.; Bolink, H. J.; Schönle, J.; Graber, S.; Housecroft, C. E.; Constable, E. C.; Zampese, J. A. Copper(I) Complexes for Sustainable Light-Emitting Electrochemical Cells. *J. Mater. Chem.* **2011**, *21* (40), 16108–16118.

(45) Fresta, E.; Volpi, G.; Milanesio, M.; Garino, C.; Barolo, C.; Costa, R. D. Novel Ligand and Device Designs for Stable Light-Emitting Electrochemical Cells Based on Heteroleptic Copper(I) Complexes. *Inorg. Chem.* **2018**, *57* (16), 10469–10479.

(46) Weber, M. D.; Viciano-Chumillas, M.; Armentano, D.; Cano, J.; Costa, R. D. σ-Hammett Parameter: A Strategy to Enhance Both Photo- and Electro-Luminescence Features of Heteroleptic Copper(I) Complexes. *Dalt. Trans.* **2017**, *46* (6312), 6312–6323.

(47) Hoertz, P. G.; Staniszewski, A.; Marton, A.; Higgins, G. T.; Incarvito, C. D.; Rheingold, A. L.; Meyer, G. J. Toward Exceeding the Shockley-Queisser Limit: Photoinduced Interfacial Charge Transfer Processes That Store Energy in Excess of the Equilibrated Excited State. *J. Am. Chem. Soc.* **2006**, *128* (25), 8234–8245.

(48) Meier, S. B.; Hartmann, D.; Winnacker, A.; Sarfert, W. The Dynamic Behavior of Thin-Film Ionic Transition Metal Complex-Based Light-Emitting Electrochemical Cells. *J. Appl. Phys.* **2014**, *116* (10), 104504.

(49) Munar, A.; Sandström, A.; Tang, S.; Edman, L. Shedding Light on the Operation of Polymer Light-Emitting Electrochemical Cells Using Impedance Spectroscopy. *Adv. Funct. Mater.* **2012**, *22* (7), 1511–1517.

(50) Brug, G. J.; Van den Eeden, A. L. G.; Sluyters-Rehbach, M.; Sluyters, J. H. The Analyis of Electrode Impedances Complicated by the Presence of a Constant Phase Element. *J. Electroanal. Chem. Interfacial Electrochem.* **1984**, *176* ((1-2)), 275–295.

(51) Hirschorn, B.; Orazem, M. E.; Tribollet, B.; Vivier, V.; Frateur, I.; Musiani, M. Determination of Effective Capacitance and Film Thickness from Constant-Phase-Element Parameters. *Electrochim. Acta* **2010**, *55* (21), 6218–6227.

(52) Kaeser, A.; Mohankumar, M.; Mohanraj, J.; Monti, F.; Holler, M.; Cid, J.-J.; Moudam, O.; Nierengarten, I.; Karmazin-Brelot, L.; Duhayon, C.; et al. Heteroleptic Copper(I) Complexes Prepared from Phenanthroline and Bis-Phosphine Ligands. *Inorg. Chem.* **2013**, *52* (20), 12140–12151.

(53) Nishikawa, M.; Sawamura, S.; Haraguchi, A.; Morikubo, J.; Takao, K.; Tsubomura, T. Highly Emissive Copper(i) Complexes Bearing Diimine and Bis(Diphenylphosphinomethyl)-2,2-Dimethyl-1,3-Dioxolane. *Dalt. Trans.* **2015**, *44* (1), 411–418.

(54) Keller, S.; Constable, E. C.; Housecroft, C. E.; Neuburger, M.; Prescimone, A.; Longo, G.; Pertegás, A.; Sessolo, M.; Bolink, H. J. [Cu(Bpy)(P^P)] + Containing Light-Emitting Electrochemical Cells: Improving Performance through Simple Substitution. *Dalt. Trans.* **2014**, *43* (44), 16593–16596.

(55) Zhang, Q.; Ding, J.; Cheng, Y.; Wang, L.; Xie, Z.; Jing, X.; Wang, F. Novel Heteroleptic CuI Complexes with Tunable Emission Color for Efficient Phosphorescent Light-Emitting Diodes. *Adv. Funct. Mater.* **2007**, *17* (15), 2983–2990.

(56) Armaroli, N.; Accorsi, G.; Cardinali, F.; Listorti, A. *Photochemistry and Photophysics of Coordination Compounds: Copper*; Balzani, V., Campagna, S., Eds.; Springer Berlin Heidelberg, 2007; Vol. 280.

(57) Nishikawa, M.; Sawamura, S.; Haraguchi, A.; Morikubo, J.; Takao, K.; Tsubomura, T. Highly Emissive Copper(I) Complexes Bearing Diimine and Bis(Diphenylphosphinomethyl)-2,2-Dimethyl-1,3-Dioxolane. *Dalt. Trans.* **2015**, *44* (1), 411–418.

(58) McCusker, C. E.; Castellano, F. N. Design of a Long-Lifetime, Earth-Abundant, Aqueous Compatible Cu(I) Photosensitizer Using Cooperative Steric Effects. *Inorg. Chem.* **2013**, *52* (14), 8114–8120.

(59) Andrés-Tomé, I.; Fyson, J.; Baiao Dias, F.; Monkman, A. P.; Iacobellis, G.; Coppo, P. Copper(I) Complexes with Bipyridyl and Phosphine Ligands: A Systematic Study. *Dalt. Trans.* **2012**, *41* (28), 8669–8674.

(60) Costa, R. D.; Ortí, E.; Bolink, H. J.; Graber, S.; Housecroft, C. E.; Neuburger, M.; Schaffner, S.; Constable, E. C. Two Are Not Always Better than One: Ligand Optimisation for Long-Living Light-Emitting Electrochemical Cells. *Chem. Commun.* **2008**, No. 15, 2029–2031.

(61) Moudam, O.; Kaeser, A.; Delavaux-Nicot, B.; Duhayon, C.; Holler, M.; Accorsi, G.; Armaroli, N.; Séguy, I.; Navarro, J.; Destruel, P.; et al. Electrophosphorescent Homo- and Heteroleptic Copper(I) Complexes Prepared from Various Bis-Phosphine Ligands. *Chem. Commun. (Camb).* **2007**, *3092* (29), 3077–3079.

(62) Zhang, L.; Li, B.; Su, Z. Realization of High-Energy Emission from [Cu (N-N)(P-P)] +

Complexes for Organic Light-Emitting Diode Applications. **2009**, *113*, 13968–13973.

(63) Che, G.; Su, Z.; Li, W.; Chu, B.; Li, M.; Hu, Z.; Zhang, Z. Highly Efficient and Color-Tuning Electrophosphorescent Devices Based on Cu[Sup I] Complex. *Appl. Phys. Lett.* **2006**, *89* (10351), 103511.

(64) Bastatas, L. D.; Moore, M. D.; Slinker, J. D. The Effect of the Dielectric Constant and Ion Mobility in Light-Emitting Electrochemical Cells. *Chempluschem* **2017**, *83*, 266–273.

(65) Costa, R. D.; Ortí, E.; Bolink, H. J. Recent Advances in Light-Emitting Electrochemical Cells. *Pure Appl. Chem.* **2011**, *83* (12), 2115–2128.

(66) Mindemark, J.; Edman, L. Illuminating the Electrolyte in Light-Emitting Electrochemical Cells. *J. Mater. Chem. C* **2016**, *4* (3), 420–432.

(67) Xu, J.; Sandström, A.; Lindh, E. M.; Yang, W.; Tang, S.; Edman, L. Challenging Conventional Wisdom: Finding High-Performance Electrodes for Light-Emitting Electrochemical Cells. *ACS Appl. Mater. Interfaces* **2018**, *10* (39), 33380–33389.

(68) Höfle, S.; Lutz, T.; Egel, A.; Nickel, F.; Kettlitz, S. W.; Gomard, G.; Lemmer, U.; Colsmann, A. Influence of the Emission Layer Thickness on the Optoelectronic Properties of Solution Processed Organic Light-Emitting Diodes. *ACS Photonics* **2014**, *1* (10), 968–973.

(69) Kalyuzhny, G.; Buda, M.; Mcneill, J.; Barbara, P.; Bard, A. J. Stability of Thin-Film Solid-State Electroluminescent Devices Based on Tris (2 , 2 ′ -Bipyridine) Ruthenium (II) Complexes. *J. Am. Chem. Soc.* **2003**, *125* (Ii), 6272–6283.

(70) Fresta, E.; Volpi, G.; Garino, C.; Barolo, C.; Costa, R. D. Contextualizing Yellow Light-Emitting Electrochemical Cells Based on a Blue-Emitting Imidazo-Pyridine Emitter. *Polyhedron* **2018**, *140*, 129–137.

SYNOPSIS. The first Cu(I)-based deep-red emitting LECs were achieved with $[Cu(N^N)(P^P)]^+$ complexes. Upon changing the P^P ligand, deep-red emitting devices with high irradiances of up to 97.9 µW/cm^2, long stabilities of up to 21 h and an excellent color stability (x/y of 0.66 / 0.32) were realized. More important, we carefully study the electroluminescent behavior with respect to the irradiance, light output, color quality and stability, as well as the impact of introducing an ionic liquid as a supporting electrolyte. Finally, we tuned the device color by mixing a wide band-gap material that led to white-emitting devices with CIE 1931 color coordinates of x/y of 0.31 / 0.32 and a high color rendering index (CRI) of 92.

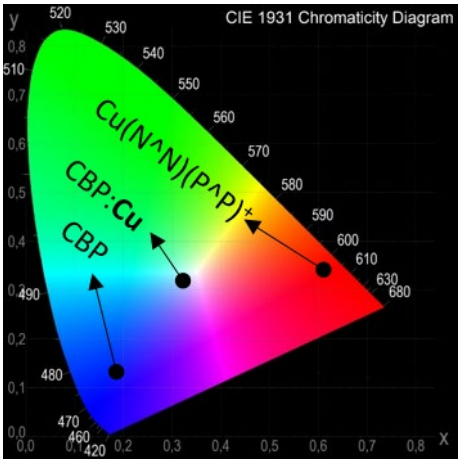

(1st proposition)

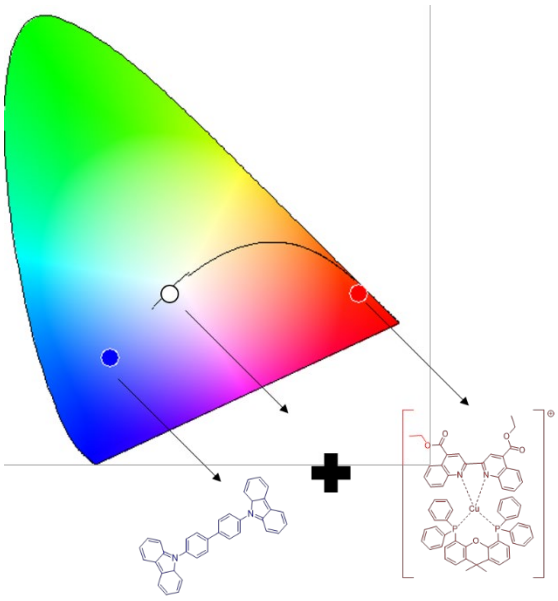

(2nd proposition)